Potential-Well Distortion in Barrier RF

C.M. Bhat and K.Y. Ng
FNAL, Batavia, IL 60510, USA

Head-tail asymmetry has been observed in the longitudinal beam profiles in the Fermilab Recycler Ring where protons or antiprotons are stored in rf barrier buckets. The asymmetry is caused by the distortion of the rf potential well in the presence of resistive impedance. Gaussian energy distribution can fit the observed asymmetric beam profile but not without discrepancy. It can also fit the measured energy distribution. On the other hand, generalized elliptic distribution gives a better fit to the beam profile. However, it fails to reproduce the observed energy distribution.

1. INTRODUCTION

Head-tail asymmetry of the longitudinal beam profile has been observed at the SLAC SLC damping ring [1] and in other electron rings. This is attributed to the distortion of the rf potential by the resistive part of the coupling impedance, and the experimental measurement at the SLC damping ring, depicted in Figure 1, fits the theory very well. However, such an asymmetry has never been reported in proton bunches.

In the presence of a pure resistive impedance R_s, the potential-well distorted bunch profile of an electron bunch, $\rho(\tau)$, can be obtained from the solution of the Haissinski equation [2], which states

$$\rho(\tau) = \rho_0 \exp\left[-\frac{\tau^2}{2\sigma_\tau^2} + \alpha_{_R} N \int_0^\tau \rho(\tau')d\tau'\right] \ , \qquad (1)$$

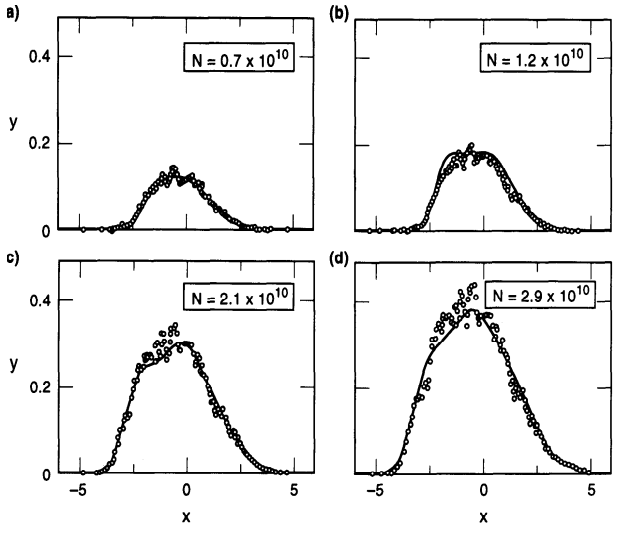

Figure 1: Potential-well distortion of bunch shape for various beam intensities for the SLAC SLC damping ring. Solid curves are solutions of the Haissinski equation and open circles are measurements. The horizontal axis is $x = \tau/\sigma_\tau$, in units of unperturbed rms bunch length, while the vertical axis gives $y = 4\pi e\rho(\tau)/[V'_{\rm rf}(0)\sigma_\tau]$, where $V'_{\rm rf}(0)$ is the rf potential gradient at $x = 0$. The beam is going to the left.

where τ is the arrival time (positive/negative for the head/tail), σ_τ is the rms bunch length in the absence of the impedance, ρ_0 is the longitudinal density of the beam center,

$$\alpha_{_R} = \frac{e^2\beta^2 E_0 R_s}{\eta T_0 \sigma_E^2} \ , \qquad (2)$$

βc is the particle velocity with c being the velocity of light, η is the slip factor, N is the number of particles in the bunch each carrying the electron charge e, E_0 is the beam nominal energy, and $\sigma_{_E}$ is the unperturbed rms energy spread. The equation can be solved in the closed form giving a shift of the profile peak from the center

$$\Delta\tau = \frac{\alpha_{_R} N \sigma_\tau}{\sqrt{2\pi}} \ . \qquad (3)$$

The potential-well distorted beam profiles for various resistive impedance are shown in Figure 2.

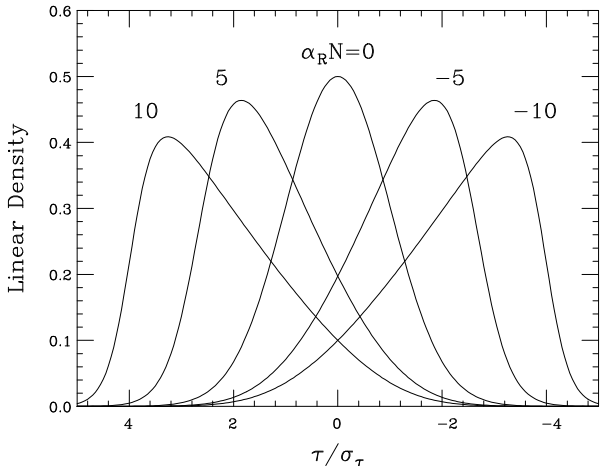

Figure 2: Exact longitudinal beam profile solution of the Haissinski equation when the impedance is purely resistive. The parameter $\alpha_{_R} N$, defined in Eq. (2), is proportional to the resistive impedance R_s and the beam intensity, and is positive above transition and negative below transition. The beam is going to the left. Its profile lags backward below transition because of resistive loss, and leans forward above transition because particles with smaller energy travel faster above transition.

Notice that the first term in the exponent of Eq. (1), $U_{\rm rf}(\tau) = -\tau^2/(2\sigma_\tau^2)$, represents the linearized rf potential and is an even function of the particle arrival time τ, while the second term, $\sim \alpha_{_R} N\rho_0\tau$, the cause of the asymmetric solution, is an odd function of τ, representing the perturbation to the rf potential arising from the interaction of the beam with the resistive impedance. The reactive part of the coupling impedance, on the other hand, distorts the rf potential symmetrically and therefore contributes only to the lengthening and shortening of the beam. The longitudinal asymmetry of the beam is only significant, however, when the second term is comparable to the first term. Proton beams are usually long and the bunch spectra roll off before they reach the broadband resonance. In other words, proton beams can hardly see the real part of the impedance. Thus the effective $\alpha_{_R} N/\sqrt{2\pi}$ is usually very small and, as a result, no significant head-tail asymmetry has ever been reported. However, at the Fermilab Recycler Ring where rf barriers are used [3], the rf potential experienced by most part of the beam is essentially zero. For this reason, head-tail asymmetry of the beam profile has been observed.

2. THE RECYCLER RF

Broadband cavities are employed to create barriers of opposite polarities to confine antiprotons [4]. Some of the merits are:

1. The beam can spread out uniformly, as indicated in the top plot of Figure 3, so that the space-charge force becomes smaller.
2. Two batches can be merged easily by moving them in two separate barrier buckets close together and then annihilating the two central barriers, as indicated in the lower plot of Figure 3.
3. The length of a batch can be compressed by moving the two barriers closer together slowly.
4. The whole batch can be moved from one location to another by moving the two confining barriers slowly in the same direction.

The are four 50 Ω broadband ferrite-loaded rf stations [4]. The amplifiers are of 3.5 kW from 10 kHz to 100 MHz, capable of supplying a total of ±2 kV. The rf waveform generated is determined by the amplitude and phase of each of the 588 revolution harmonics.

When the baseline between the two barrier pulses is nonzero, as shown in the top plot of Figure 4, the barrier potential becomes slanting, as shown in the lower plot. Such nonzero baseline can come from either rf errors or the coupling impedance of the vacuum chamber. Here, we are talking about a deviation of ~ 10 V from zero, out of a total barrier voltage of ±2 kV, or $\sim 0.5\%$.

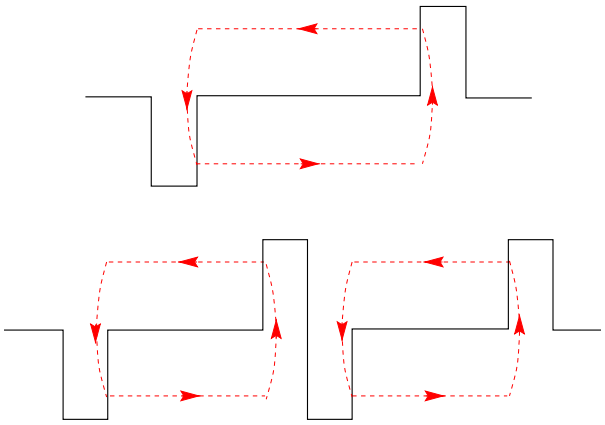

Figure 3: Top: The trajectory of a proton inside a barrier bucket set up by two barrier waves with equal and opposite polarities. Bottom: Two barrier buckets set up by 4 barrier waves are prepared side-by-side. When the two central barrier waves annihilate each other, the two buckets will be merged into one.

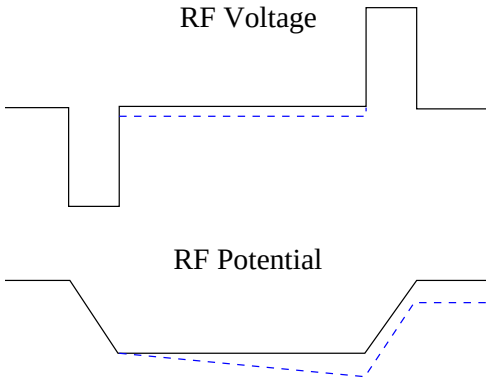

Figure 4: When the baseline voltage (top) inside a barrier bucket set up by two barrier waves of opposite polarities is different from zero (dashed), the rf potential well (bottom) no longer has a flat bottom. A beam inside the potential well therefore no longer has a head-tail symmetric linear density.

2.1. Nonlinearity in High-Level RF

In the top plot of Figure 5, head-tail asymmetry is evident for the proton beam in a barrier bucket at the low intensity of $\sim 1 \times 10^{11}$ with the beam profile leaning towards the head, which is the left in the display. The Recycler Ring is a permanent-magnet storage ring at 8.9383 GeV operating below transition. Since the beam leans forwards, it cannot be because of the interaction with the resistive coupling impedance, because particles losing energy will lag behind below transition.

After some investigation, a small parasitic 90 kHz (revolution harmonic component) sinusoidal component was found imposed on the rf vector sum of all four rf stations [5]. This is equivalent to having a

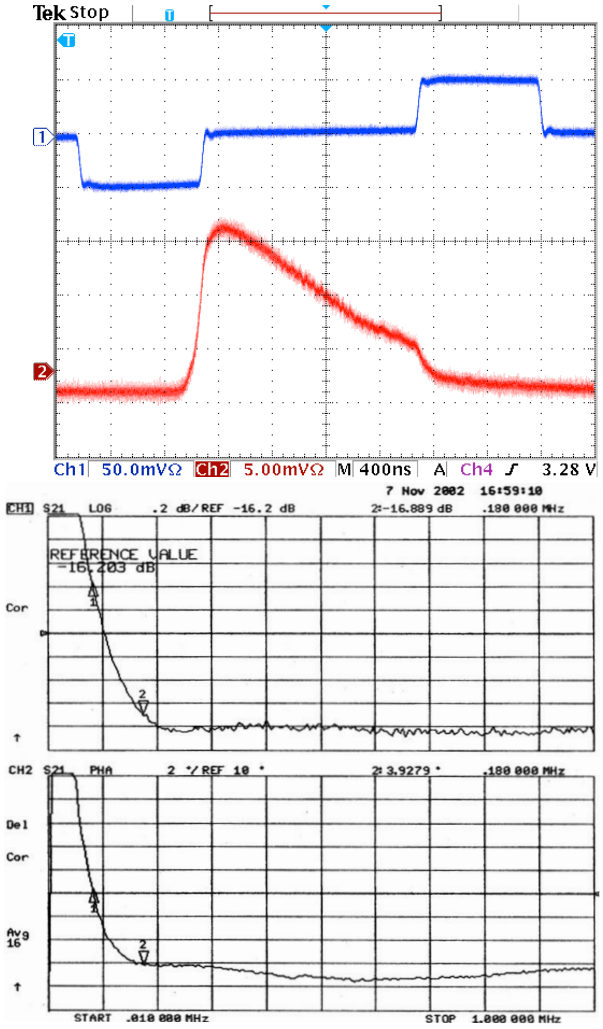

Figure 5: Top: A beam of intensity $\sim 1 \times 10^{11}$ exhibits head-tail asymmetry between two barrier waves. Middle and bottom: Amplitude and phase in the Recycler high-level rf exhibit nonlinearity from 90 kHz to 1 MHz. The amplitude plot is 0.2 dB per division and the phase plot is 2° per division. Markers 1 and 2 are at fundamental ($\sim$ 90 kHz) and first ($\sim$ 180 kHz) revolution harmonics. A response with flatness of less than 0.26 dB in amplitude and less than 1.8° in phase is required.

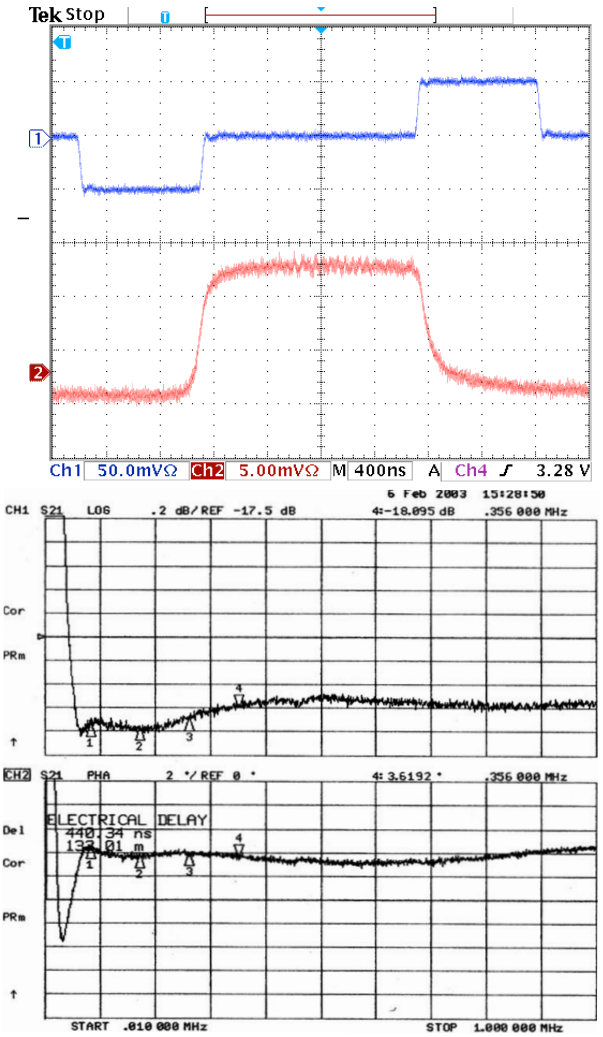

Figure 6: Top: After the implementation of the linearization transfer function, head-tail asymmetry in beam disappears. Middle and bottom: Amplitude and phase in the Recycler high-level rf are now consistent with the linearity requirement. The amplitude plot is 0.2 dB per division and the phase plot is 2° per division. Markers 1, 2, 3, and 4 are at fundamental ($\sim$ 90 kHz), first ($\sim$ 180 kHz), second, and third revolution harmonics.

nonlinear response in the high-level rf amplifiers. The design requires the response for all revolution components from 90 kHz to 1 MHz to differ by less than 0.26 dB in amplitude and 1.8° in phase. As is displayed in the middle and lower plots of Figure 5, the S-parameter S_{21} measurement reveals a much larger deviation from linearity for the parasitic fundamental component. Between 90 kHz (Marker 1) and 180 kHz (Marker 2), the variations are 1.1 dB in amplitude (middle plot with 0.2 dB per division) and 6.26° in phase (lower plot with 2° per division). Using a network analyzer, S_{21} was realized for the overall system, and from mathematical modeling, a second order numerator and denominator transfer function was found. The inverse of this transfer function provides the required linearization transfer function. The linearization transfer function was realized in hardware by summing high-pass, band-pass, and low-pass filters together [6]. Implementation of the correction brings the response of the high-level rf to the required linearization, as demonstrated in the middle and lower plots of Figure 6. As expected, the head-tail asymmetry in the beam profile, shown in the top plot, disappears.

3. COUPLING IMPEDANCE

With the linearization compensation properly adjusted for beams with low intensities ($\sim 1 \times 10^{11}$),

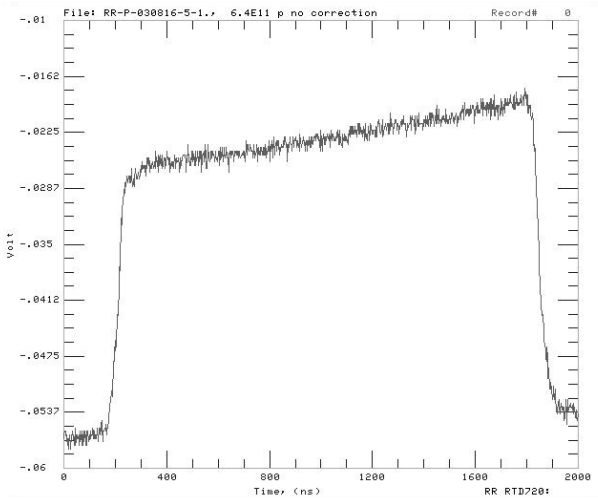

Figure 7: A beam of intensity $N = 6.4 \times 10^{11}$ inside a barrier bucket of width ~ 1.59 μs exhibits head-tail asymmetry, after response linearization is implemented. The beam lags backwards in agreement with energy loss due to resistive impedance.

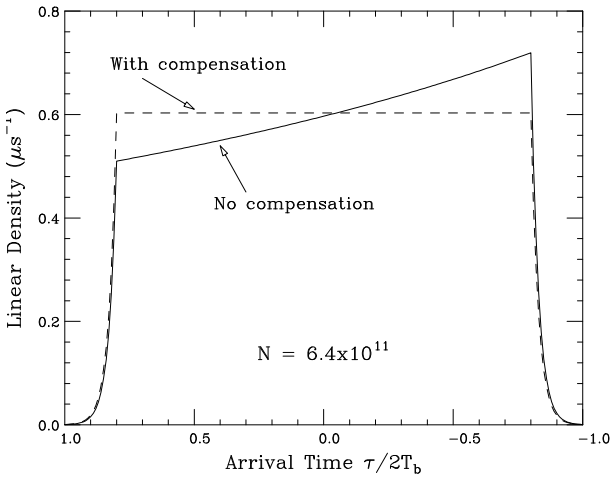

Figure 8: Solution of the Haissinski equation [Eq. (9) below] with a resistive impedance of $R_s = 200$ Ω and beam intensity 6.4×10^{11} reproduces the observed beam profile with head-tail asymmetry shown in Figure 7. A compensating voltage, 12.4 V, restores the head-tail symmetry. Here T_b is total bunch length.

the slant in the beam profile reappears, however, in beams with higher beam intensities. An example is shown in Figure 7 at the intensity of 6.4×10^{11}. Unlike the asymmetry seen in Figure 5, now the tail lags behind the head. Since the Recycler Ring operates below transition, this asymmetry may come from the interaction with the resistive part of the longitudinal impedance.

The barrier broadband cavities have a total resistive impedance $\mathcal{R}e\, Z_0^{\parallel} = 200\ \Omega$, which is visible to the beam up to ~ 45 MHz (or up to revolution harmonics 500). Comparatively, the resistive wall impedance of the vacuum chamber can be neglected because its real part is only $\mathcal{R}e\, Z_0^{\parallel} = 12.0\ \Omega$ at the revolution harmonic [7]. When substituted into the Haissinski equation, the solution results in a beam profile closely resembling that observed in Figure 7. This theory-predicted solution is depicted as solid in Figure 8.

The local current of the beam in between the barrier pulses is approximately

$$I_{\rm local} = \frac{eN}{T_2}\ , \qquad (4)$$

where $T_2 \approx 1.59$ μs is the distance between the inner edges of the two barriers. The beam-loading voltage left in the barrier cavities is therefore

$$V_b = I_{\rm local} Z_0^{\parallel} \approx eNZ_0^{\parallel}\rho(\tau) \approx \frac{eNZ_0^{\parallel}}{T_2} = 12.9\ {\rm V}\ . \qquad (5)$$

Thus the beam-loading effect can be compensated by adding an accelerating voltage to the broadband barrier cavities. As expected, the head-tail asymmetry disappears in Figure 8 with the addition of such a voltage. Experimentally, we also see that slant of the beam profile goes away in Figure 9 after adding ~ 8.82 V to the region between the barriers.

There have been discrepancies between the solutions of the Haissinski equation and experimental observations. If we assume the energy offset of the beam ΔE to follow a Gaussian distribution, the $R_s = 200\ \Omega$ leads to a solution of the beam profile $\rho(\tau)$ at the intensity 6.4×10^{11} with a head-tail asymmetry of $\pm 17\%$, which is larger than what we actually observe[1]

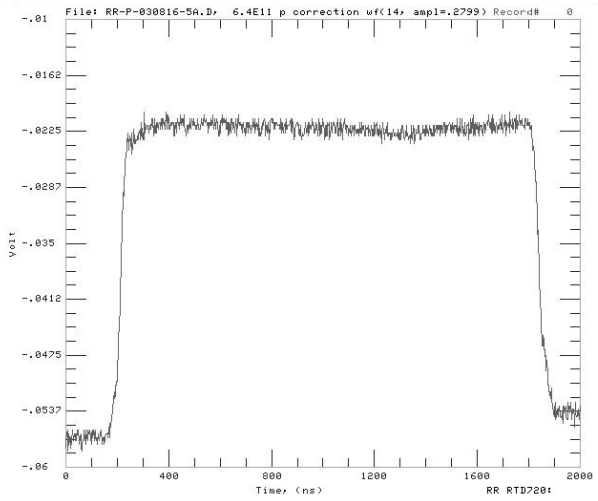

Figure 9: The head-tail asymmetry of the beam profile in Figure 7 is compensated by adding ~ 8.82 V to the region between the barriers.

[1]The fractional asymmetry is not so well-defined in Figure 7 and in other measurements, because the baselines at the head and the tail differ by s significant amount.

($\sim 14\%$) in Figure 7. To correct for asymmetry in the Haissinski equation, one needs 12.4 V, which is $\sim 40\%$ larger than actual compensation needed in Figure 9.

We end this section by plotting some particle trajectories in the longitudinal phase space in Figure 10. We see that the trajectories in the presence of beam loading, regardless of going to the left or right, are always losing energy. It is obvious that when integrating over energy offset, the beam profile will have a higher density near the tail than the head.

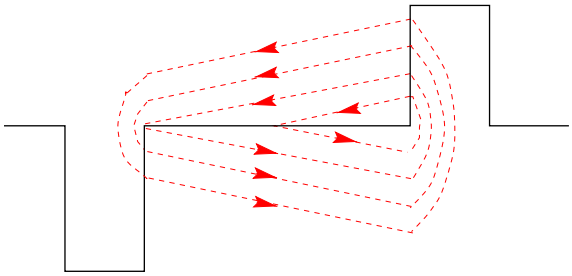

Figure 10: A schematic drawing of the trajectories of particles inside a barrier bucket interacting with a resistive impedance. Because of a constant loss of energy along the trajectories, the longitudinal profile of the beam exhibits higher density at the tail than the head.

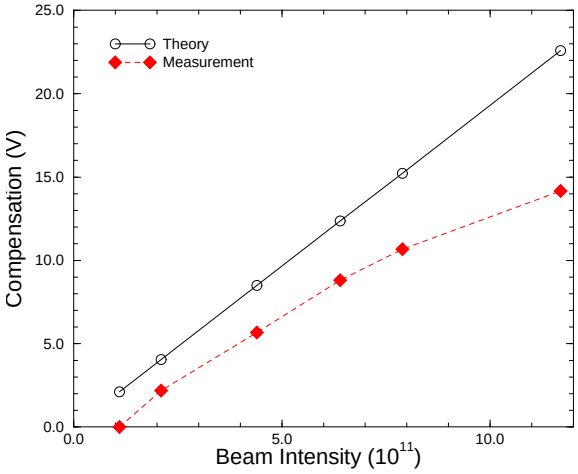

Figure 11: The compensating voltage is shown as a function of the beam intensity, theory in circles and experimental observation in solid rhombuses. The experimental compensating voltages are consistently less than the theoretical prediction.

4. UNSOLVED PROBLEMS

There remain many unsolved problems in this analysis of head-tail asymmetry in the longitudinal profile of the beam inside a barrier bucket. Some of them are listed below:

4.1. Problem 1

The theory-predicted voltage compensation is in general larger than what is needed in reality. The theory predictions are depicted as open circles and joined by solid lines in Figure 11. The experimental required compensation voltages are plotted as solid rhombuses and joined by dashes. The deviation appears to grow larger at higher intensities. Some possible reasons for this discrepancy are:

1. The linearization of the high-level rf amplifier response has been over-compensated. During the experimental measurement of the beam profile, the linearization knobs have been adjusted with the intention to eliminate the slant of the profile when the beam intensity is at 1.1×10^{11}. The over-compensation of linearity will definitely lead to less head-tail asymmetry at higher beam intensities.

2. The shunt impedance of the cavities may have been less than 200 Ω. However, loaded shunt impedance may not be much less than the unloaded shunt impedance because the cavities are broadband. It will be nice if the loaded impedance can be measured independently.

   It is possible that the impedance model used in the Haissinski equation is incorrect. So far we have assumed a resistive impedance R_s which is frequency independent. In reality, the shunt impedance of the broadband cavities is visible to the beam up to 45 MHz only and becomes negligible at higher frequencies. To simulate this frequency dependency, we try to introduce a more realistic model for the longitudinal wake,

$$W_0(t) = \sqrt{\frac{2}{\pi}} R_s \sigma_\omega e^{-\sigma_\omega^2 t^2/2} \ , \qquad (6)$$

   for a particle lagging behind a point source by the time t, so that the resistive impedance

$$\mathcal{R}e\, Z_0^{\parallel}(\omega) = R_s e^{-\omega^2/(2\sigma_\omega^2)} \qquad (7)$$

   rolls off around $\sigma_\omega/2\pi \approx 45$ MHz. Unfortunately, this wake only leads to negligible changes in our results, which are to be expected, because the beam inside a barrier bucket does not have many high-frequency components.

It is important to point out that the theoretical determination of the slant compensating voltage is, in fact, very general. It depends only on the fact that the distribution $\psi(\Delta E, \tau)$ in longitudinal phase space is a function of the Hamiltonian H, or

$$\psi(\Delta E, \tau) = \psi(H) \ , \qquad (8)$$

and does not depend on the detailed beam distribution in the longitudinal phase space.

4.2. Problem 2

The observed longitudinal head-tail asymmetric beam profiles have been very linear, even up to the intensity of 11.8×10^{11}, as illustrated in the top plot of Figure 12. On the other hand, the predicted head-tail asymmetry, as depicted in the lower plot, is not linear.

In the presence of a barrier rf and a purely resistive coupling impedance the Haissinski equation can be written as

$$\rho(\tau) = \rho_0 \exp\left[-\frac{2\pi\beta^2 E_0 e V_0 T_1}{|\eta|\sigma_E^2 T_0} U_{\rm rf}(\tau) + \alpha_{_R} N \int_0^\tau \rho(\tau')d\tau'\right] , \qquad (9)$$

where T_0 is the revolution period and $\pm V_0$ is the voltage of the squared barriers with time duration T_1. Here, $U_{\rm rf}$ is the reduced rf barrier potential, something as indicated as solid drawing in the lower plot of Figure 4 with negative and positive unit voltage gradients at the squared barriers.

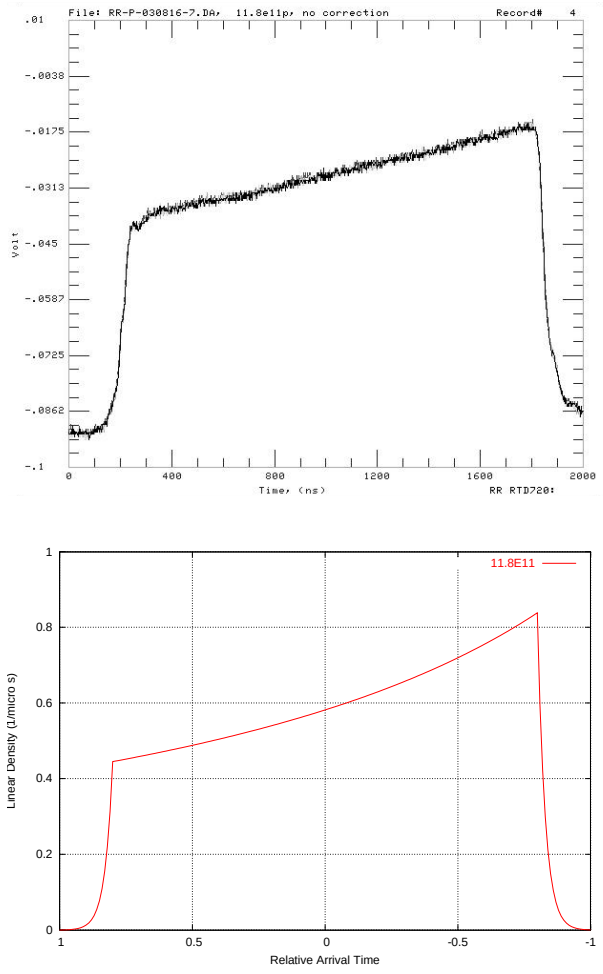

Figure 12: The observed longitudinal profile of a 11.8×10^{11} beam in the top plot is very linear, whereas the theoretical predicted profile assuming Gaussian energy distribution in the lower plot is not.

The beam profile $\rho(\tau)$ can be solved more easily by converting the Haissinski integral equation into a differential equation. In between the barriers, where potential $U_{\rm rf}(\tau) = 0$, differentiation with respect to τ gives

$$\rho' = -\alpha_{_R} N \rho^2 \ . \qquad (10)$$

The solution of this differential equation is

$$\rho(\tau) = \frac{\rho_0}{1 + \alpha_{_R} N \rho_0 \tau} \ , \qquad (11)$$

which is just the solution of the Haissinski equation in the region between the barrier waves. We can see clearly that the beam profile is, in fact, hyperbolic instead of linear.

So far we have assumed a Gaussian energy distribution of the beam. We can also try the more generalized elliptical-like distribution. In the absence of any rf and coupling impedance, the distribution in the longitudinal phase space is

$$\psi(\tau, \Delta E) = A\left[\widehat{\Delta E}_0^{\,2} - \Delta E^2\right]^n \ , \qquad (12)$$

where $\widehat{\Delta E}_0$ is the half-energy spread, A is a normalization constant, and n is a number that need not be an integer or half integer. In the presence of two barriers and a pure resistive impedance R_s, the Hamiltonian can be written as

$$H = -\frac{\eta(\Delta E)^2}{2\beta^3 c E_0} - \frac{eV_0 T_1}{\beta c T_0} U_{\rm rf}(\tau) + \frac{e^2 R_s N}{\beta c T_0}\int_0^\tau d\tau' \rho(\tau') \ . \qquad (13)$$

The phase-space distribution, being a function of the Hamiltonian, therefore transforms from Eq. (12) to

$$\psi(\tau, \Delta E) = A\left[\widehat{\Delta E}_0^{\,2} - \widehat{\Delta E}_0^{\,2}\left(\frac{\Delta E^2}{\widehat{\Delta E}_0^{\,2}} - bU_{\rm rf}(\tau) + a\int_0^\tau \rho(\tau')d\tau'\right)\right]^n , \qquad (14)$$

where

$$a = \frac{2\beta^2 e^2 N E_0 R_s}{-\eta T_0 \widehat{\Delta E}_0^{\,2}} \quad \text{and} \quad b = \frac{2\beta^2 E_0 e V_0 T_1}{-\eta T_0 \widehat{\Delta E}_0^{\,2}} \ . \qquad (15)$$

We can rewrite the above in the simpler form

$$\psi(\tau, \Delta E) = A\left[\widehat{\Delta E}^{\,2}(\tau) - \Delta E^2\right]^n \ , \qquad (16)$$

with

$$\widehat{\Delta E}^{\,2}(\tau) = \widehat{\Delta E}_0^{\,2}\left[1 + bU_{\rm rf}(\tau) - a\int_0^\tau \rho(\tau')d\tau'\right] . \qquad (17)$$

Then the longitudinal beam profile can be readily obtained by an integration over the energy offset,

$$\rho(\tau) = 2A\left[\widehat{\Delta E}^2(\tau)\right]^{n+\frac{1}{2}} \times \\ \times \int_0^1 (1-t^2)^n dt = 2\gamma_n A\left[\widehat{\Delta E}^2(\tau)\right]^{n+\frac{1}{2}}, \quad (18)$$

where

$$\gamma_n = \int_0^1 (1-t^2)^n dt = \frac{\pi\Gamma(2n+2)}{2^{2n+1}\Gamma^2\left(n+\frac{3}{2}\right)} . \quad (19)$$

We next consider the region $-\frac{1}{2}T_2 \le \tau \le \frac{1}{2}T_2$ where the barrier potential $U_{\rm rf}(\tau) = 0$ with T_2 representing the separation between the inner edges of the barriers. Differentiation with respect to τ leads to

$$\rho' = -\frac{2n+1}{2}\, a\rho_0^{\frac{2}{2n+1}}\rho^{\frac{4n}{2n+1}} , \quad (20)$$

where

$$\rho_0 = 2\gamma_n A\left(\widehat{\Delta E_0}^2\right)^{n+\frac{1}{2}} \quad (21)$$

is the linear density at $\tau = 0$. This differential equation can be integrated easily resulting in the beam profile

$$\rho(\tau) = \rho_0\left[1+\frac{2n-1}{2}\, a\rho_0\tau\right]^{-\frac{2n+1}{2n-1}} . \quad (22)$$

The integration from $\tau = -\frac{1}{2}T_2$ to $+\frac{1}{2}T_2$ should give unity, or

$$\int \rho(\tau)d\tau = \frac{1}{a}\left[\left(1-\frac{2n-1}{2}\,\frac{a\rho_0 T_2}{2}\right)^{-\frac{2}{2n-1}} \right. \\ \left. -\left(1+\frac{2n-1}{2}\,\frac{a\rho_0 T_2}{2}\right)^{-\frac{2}{2n-1}}\right] = 1 , \quad (23)$$

from which ρ_0 and therefore the normalization constant A can be solved. Note that we should expect roughly $\rho_0 T_2 = 1$ and deviation occurs when $\rho(\tau)$ deviates from linearity. Knowing ρ_0, we can compute the maximum and minimum half energy spreads:

$$\Delta E_{\rm max,min} = \widehat{\Delta E_0}\left(1 \mp \frac{2n-1}{2}\,\frac{a\rho_0 T_2}{2}\right)^{-\frac{1}{2n-1}} , \quad (24)$$

occurring at $\tau = \pm\frac{1}{2}T_2$. The situation of $n = \frac{1}{2}$ needs special treatment, and it corresponds to an exponential distribution for the beam profile. The beam profiles corresponding to the generalized elliptical distribution of $n = 0.1$, 0.5, 1, and 1.5 are computed for beam intensity 11.8×10^{11}, half energy spread at the beam center $\widehat{\Delta E_0} = 3.8$ MeV, and resistive impedance $R_s = 200\ \Omega$. They are depicted in Figure 13. The beam profile for the Gaussian distribution with rms energy spread $\sigma_{_E} = 2.3$ MeV is also plotted for comparison, and is found to lie in between the ones corresponding to $n = 0.5$ (dashes) and $n = 1$ (dot-dash). We do see that the head-tail asymmetry becomes rather linear when $n \lesssim 0.5$ and therefore agrees with experimental observation.

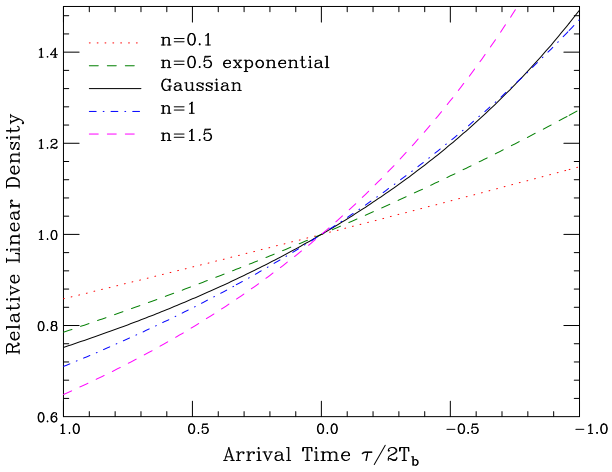

Figure 13: Longitudinal beam profile in the generalized elliptical distribution. Starting on the left from the top and going downward, the longitudinal beam profiles correspond to $n = 0.1$, $n = 0.5$ (exponential), Gaussian, $n = 1.0$, and $n = 1.5$. The predicted beam profiles are quite linear when $n \lesssim 0.5$. Here, T_b is total length of beam.

4.3. Problem 3

Although the longitudinal profile derived from the generalized elliptical distribution with $n \lesssim 0.5$ is close to linear agreeing with the observed head-tail asymmetric beam profile, the energy distribution does not agree with observation.

There is a 1.75 GHz Schottky detector in the Recycler Ring to monitor the momentum spread of the beam inside the barrier bucket. Schottky signals corresponding to beam intensity 11.67×10^{11} are depicted in Figure 14. The Schottky amplitudes are displayed in dBm which is a logarithmic scale. From this the energy distribution can be obtained easily and is shown in Figure 15 in a linear scale as solid circles joined by dots. The rms energy spread turns out to be $\sigma_{_E} = 2.3$ MeV (3.9 kHz in the Schottky-signal plot). The energy distribution derived from the elliptical distribution with $n = 0.55$ is also plotted and appears similar to a parabolic distribution (dot-dashed curve) having no tails and clearly does not fit the observation at all. The energy distribution derived from the Gaussian distribution is computed and is shown as a solid curve in the figure. It appears that this distribution fits the observation very much better.

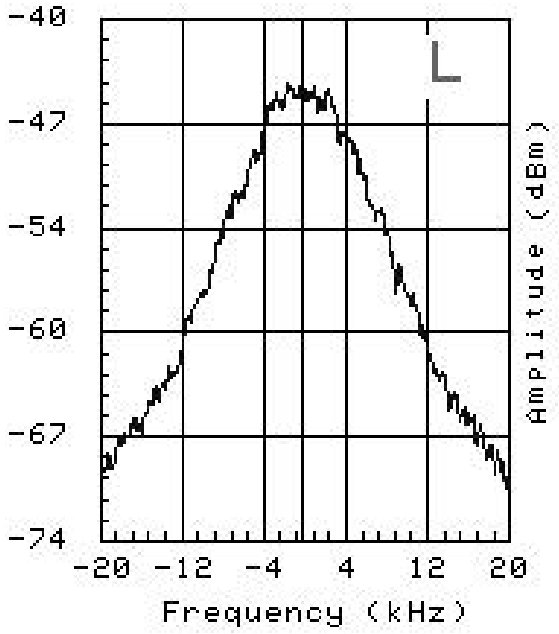

Figure 14: Schottky signals of the 19485th revolution harmonic (1.75 GHz) of a beam of intensity 11.67×10^{11} in a barrier bucket. The Schottky amplitudes are in dBm which is defined as $10 \log_{10} N_i/N_0$, where N_i is the amplitude at the ith point and N_0 is a scale factor.

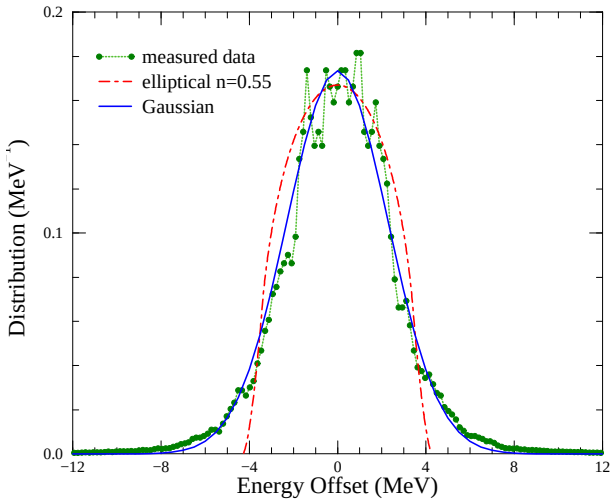

Figure 15: The Schottky signals of the beam in Figure 14 is converted into energy-offset distribution in the linear scale, and are depicted as solid circles joined by dots. The theory-predicted energy-offset distributions are also plotted for comparison. The one assuming elliptical distribution (dot-dashed) with $n = 0.55$ does not have long tails and does not fit the observed distribution well. The one assuming Gaussian energy distribution (solid) does fit the observed Schottky data well.

5. CONCLUSION

1. We have reported head-tail asymmetry in a proton beam due to potential-well distortion of the special barrier rf.

2. This beam linear density $\rho(\tau)$, being head-tail asymmetric, may overflow the barrier bucket when beam intensity is too high.

3. When barrier bucket is too full, instabilities will occur due to resonances driven by rf jitters [8].

4. The asymmetry will also affect other future applications of barrier rf, for example, in the stacking of two booster batches on top of each other in the Fermilab Main Injector in order to increase the linear density of the proton beam.

5. The required compensating beam-loading voltages appear to be smaller than what the theory predicts (Figure 11). It is important that when the beam profile is measured again in the future, proper linearization of the high-level rf is maintained. Care must be taken to assure no over-compensation of the rf response nonlinearity.

6. It appears that the generalized elliptical distribution with $n \lesssim 0.5$ leads to a rather linear beam profile and therefore fits the observation pretty well. However, the energy distribution derived from such distribution does not fit the observed one at all. On the other hand, Gaussian energy distribution fits the observed distribution rather well, but the longitudinal profile, being hyperbolic, does not fit the experimental one. Maybe we should investigate some other phase-space distributions like cosine square, etc.

Acknowledgments

Work supported by Department of Energy contract DE-AC02-76CH030000.

References

[1] Karl L.F. Bane and Ronald D. Ruth, PAC'89, Chicago, 1989, p. 789.
[2] J. Haissinski, Nuovo Cimento **18B**, 72 (1973).
[3] J. Griffin, C. Ankenbrandt, J.A. MacLachlan, A. Moretti, IEEE Trans. Nucl. Science, NS**30**, 3502 (1983); V.K. Bharadwaj, J.E. Griffin, D.J. Harding, J.A. MacLachlan, IEEE Trans. Nucl. Science NS**34**, 1025 (1987).
[4] J.E. Dey and D.W. Wildman, "Wideband Rf System for the Fermilab Recycler Ring", PAC'99, New York, 1999, p.869.

[5] J. Marriner and C.M. Bhat, private communication, 2002.
[6] J. Dey, S. Dris, T. Kubicki, J. Reid, "Linearization of the Fermilab Recycler High Level Rf", PAC'03, Portland, 2003.
[7] King-Yuen Ng, "Impedances and Beam Stability Issues of the Fermilab Recycler Ring", Fermilab Report TM-1971, 1996.
[8] S.Y. Lee and K.Y. Ng, "Particle Dynamics in Storage Rings with Barrier Rf Systems", Phys. Rev. **E55**, 5992 (1997).